Inorganic Photonic Microspheres with Localized Concentric Ordering for Deep Pattern Encoding and Triple Sensory Microsensor

Wenbin Niu, Xiao Wang, Yu Zheng, Shuwang Wu, Mutian Hua, Yunpeng Wang, Xiaohe Zhang, Alfred Iing Yoong Tok, Ximin He,* and Shufen Zhang*

Photonic microspheres offer building units with unique topological structures and specific optical functions for diverse applications. Here, a new class of inorganic photonic microspheres with superior robustness, optical and electrical properties is reported by introducing a unique localized concentric ordering architecture and chemical interaction, which further serve as building blocks for deep pattern encoding and multiple sensory optoelectronic devices. Benefiting from localized concentric ordering architecture, the resultant photonic microspheres demonstrate orientation- and angle-independent structural colors. Notably, the formation of well-combined lamellae inorganic layers by chemical interaction grants the microspheres superior mechanical robustness, excellent solvent resistance, thermal stability, and multiple optoelectronic properties simultaneously, rarely seen in previous reports. Owing to these merits, such microspheres are used to construct diverse encoded photonic patterns for anti-counterfeiting applications. Interestingly, cross-communication among neighboring microspheres creates complex photonic sub-patterns, which provide "fingerprint information" with deep encryption security. Moreover, a single photonic microsphere-based optoelectronic microsensor is demonstrated for the first time, which achieves appealing application for real-time health monitoring and safety warning toward triple environmental stimuli. This work not only provides a new kind of robust, multifunctional photonic material, but also opens a new avenue for their uses as complexed pattern encoding and multi-parametric sensing platforms.

Prof. W. B. Niu, X. Wang, Y. Zheng, Y. P. Wang,
X. H. Zhang, Prof. S. F. Zhang
State Key Laboratory of Fine Chemicals
Dalian University of Technology
West Campus, 2 Linggong Rd., Dalian 116024, China
E-mail: zhangshf@dlut.edu.cn
S. Wu, M. Hua, Prof. X. He
Department of Materials Science and Engineering
University of California
Los Angeles, CA 90095, USA
E-mail: ximinhe@ucla.edu
Prof. A. I. Y. Tok
School of Material Science and Engineering
Nanyang Technological University
Singapore 639798, Singapore

In nature, many living creatures have developed unique periodic micro- or nano-structures, well-known as photonic crystals (PC), which could interact with incident light to give rise to brilliant and non-fading structural colors for courtship, disguise, escape, and communication.[1–4] For instance, *Morpho menelaus* and *anaxibia* wings utilize the multilayer micro-concavities-based retro-reflection to exhibit bright blue and turquoise colors for mating and warning;[3,4] cephalopods possess reflecting platelets stacked in iridophores to produce iridescent colors for disguise and escape.[3,4] Inspired by these exciting natural architectures, great efforts have been devoted to developing various photonic materials with structural colors. Among them, photonic microspheres exhibit high flexibility, small size, and orientation-independent structural color because of their spherical symmetry in geometry, making them appealing for a wide range applications, including advanced photonic devices, wide viewing-angle displays,[5–9] biological sensors,[6,10–12] aesthetic pigments.[13–19] In particular, these photonic microspheres provide building blocks for constructing promising encoded patterns for complex bioassays and anti-counterfeiting,[18,20–24] and to create standalone devices for environment stimuli sensing.[23,25–27]

Conventional photonic microspheres are generally crystallized from monodispersed colloidal nanoparticles (e.g., SiO_2, polystyrene).[16,28,29] Unfortunately, the high orientation of those nanoparticles during arrangements usually causes the formation of single-crystal or multi-domain structure across the entire spherical space, resulting in non-uniform structural colors on the spherical surface.[16,21,22,28,30] A promising alternative approach for constructing photonic microspheres with uniform structural colors is to design a concentric or onion-like periodic lamellar structure like natural pearls,[26,31,32] because of its unique symmetry, fewer intrinsic defects, relatively easy prediction and control of optical properties. However, in spite of orientation-independent structural color, these concentric microspheres inevitably exhibit strong angle-dependence, which resulted from long-range ordering of the concentric lamellae in

radial orientation.[31] This angle-dependence is disadvantageous for the construction of optical materials and devices like sensors, display devices, print media and optical devices, where wide viewing angles are highly desired.[17,33] Moreover, such microspheres are usually assembled from organic molecules (e.g., block copolymers). The intrinsically low mechanical properties and relatively weak interactions (e.g., van der Waals force and hydrogen bonds) between those organic molecules lead to a low resistance to mechanical and solvent damages,[17] which make them unfavorable for long-term service in real-world applications. For example, photonic pigments must withstand various solvents and high-speed impact or particle erosion during homogenizing and painting; photonic coating has to endure various rubbing. Further, a lack of optical and electrical properties of these building materials greatly hinders their exploitation in diverse fields, such as advanced optoelectronic devices. Therefore, the development of photonic microspheres that simultaneously realize orientation- and angle-independent structural colors, mechanical robustness, solvent resistance, as well as optoelectronic properties is highly desirable.

In this work, we present the rational design and fabrication of new photonic microspheres (PCM) with the desired robustness, optical and electrical properties. First, a unique localized concentric ordering strategy is proposed to design the photonic structure, in which a concentric 1-dimensional PC shell with few periods is grown onto a rigid microsphere inner core. The onion-like concentric structure produces the orientation-independent

color, while few periods of the concentric photonic lamellae give rise to short-range ordering, thus causing the angle-independency of the structural color. On the other hand, robust, multifunctional zinc oxide and alumina are used as building materials of PC shell,[30] and are chemically grown onto the curved surface of rigid inner microcore to offer desired mechanical robustness, solvent resistance, and electrical properties.[34–39] Therefore, comparing with the conventional counterparts, the resultant photonic microspheres show not only orientation-independent and angle-independent structural colors, but also strong mechanical robustness, thermal stability, and excellent solvents tolerance. Notably, multiple optoelectronic sensing capabilities are also exhibited. As proof-of-concept, we further apply the as-prepared photonic microspheres as building units in pattern encoding for encryption and anti-counterfeiting. It is noteworthy that diverse photonic sub-patterns are exhibited through cross-communications among neighboring microspheres. Moreover, a novel single photonic microsphere-based (SPCM-based) optoelectronic microsensor is developed, which features electrical response to triple surrounding environment stimuli, showing great promise in emerging wearable electronics and smart devices. To the best of our knowledge, this is the first example of photonic crystal microsphere-based optoelectronic sensor.

The straightforward structural design and fabrication process of the photonic microspheres are shown in **Figure 1**. Photonic microspheres were prepared through growing inorganic concentric photonic structures with few periods
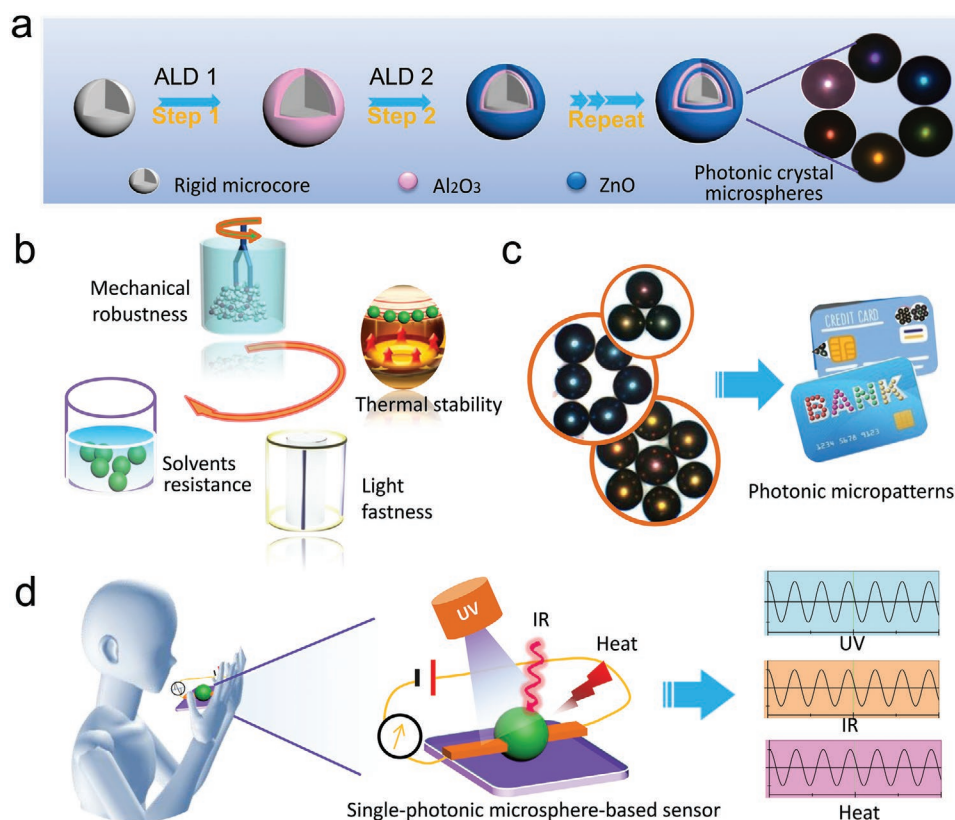

Figure 1. Schemes of inorganic concentric 1D photonic microspheres with mechanical robustness and multifunctions. Schematic diagrams of the a) preparation process and b) merits of mechanical performance of the photonic microspheres. Schematic illustrations showing their applications in c) photonic pattern encoding, and d) single particle-based microsensor with triple sensations.

**ADVANCED
SCIENCE NEWS**

www.advancedsciencenews.com

**NANO · MICRO
small**

www.small-journal.com

on glass microspheres via atomic layer deposition (ALD). To enhance the structural color saturation, here, a black glass microcore was used to reduce light absorption and incoherent scattering. A uniform photonic layer can be chemically grown by ALD through self-limiting reaction (see Experimental Section for details, and Figures S1 and S2, Supporting Information).[34–38] Trimethylaluminum, diethylzinc and deionized water were used as precursors for reaction to grow alumina and zinc oxide, respectively. An $Al(CH_3)_3$ precursor was first introduced onto the surface of the glass microspheres through self-limiting reaction with the hydroxyl groups of the glass surface to form $-O-Al-(CH_3)_2$, followed by a N_2 gas purge to remove residuals and byproducts. Subsequently, a second pulsed H_2O will react with the $Al-CH_3$ to form $Al-OH$ group, thus producing a monomolecular layer of Al_2O_3. This surface chemical reaction will result in strong chemical interaction between the deposited Al_2O_3 layer and glass substrate, thus improving the adhesion of the photonic crystal shell structure (see detailed mechanism in Figure S1, Supporting Information). Repeating the above ALD

cycle a determined number (400) yielded a layer of Al_2O_3 with ≈60 nm thickness. To grow the ZnO layer, $Zn(C_2H_5)_2$, as Zn precursor, was pulsed into deposition chamber and reacted with the as-formed outmost –OH group on the Al_2O_3 surface to produce $-O-Zn-C_2H_5$ followed by a second pulse of H_2O after N_2 purge (see detailed mechanism in Figure S2, Supporting Information). Next, the concentric photonic structure was constructed by alternately depositing Al_2O_3/ZnO lamellae twice. To develop photonic microspheres with distinct structural colors, the optical thicknesses of ZnO layers were simply and effectively adjusted by the number of ALD cycles, while the Al_2O_3 layer remained. The corresponding PCs are denoted as PCM-I to PCM-VI (see Experimental Section in Supporting Information), respectively.

This unique morphology and structure are characterized by scanning electron microscopy (SEM). Evidently, the obtained photonic microspheres maintain the uniform spherical morphology of the original glass core well, as demonstrated in **Figure 2**a at low magnification. Cross-sectional SEM images observed from the cut reveals that the surface is covered by a
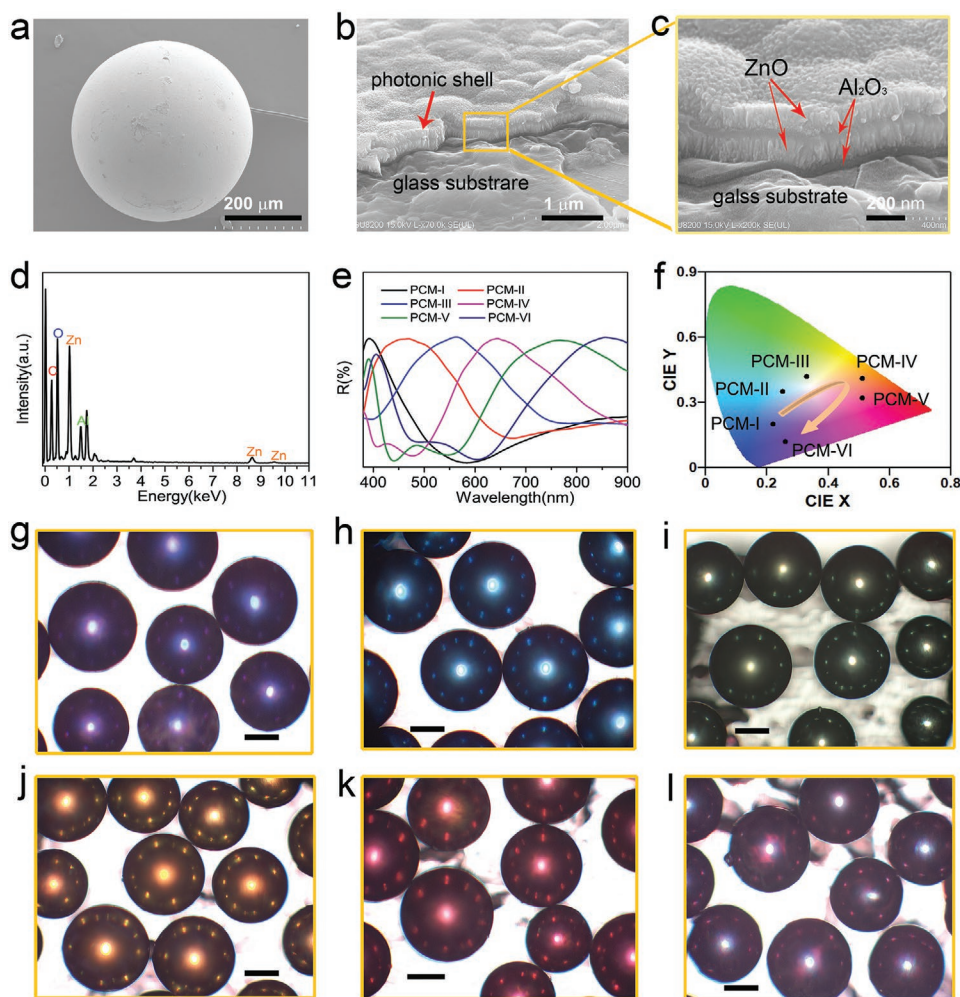

Figure 2. Microstructures and optical properties of inorganic 1D photonic microspheres. SEM images showing a) a single photonic microsphere (PCM-VI) and its cross-section at b) low- and c) high-magnification observed by cutting it apart with a blade. d) Energy-dispersive X-ray spectrum revealing relative content of elements in PCM-V. e) Normalized reflectance spectra and f) corresponding CIE chromaticity diagram of structurally colored microspheres. Optical microscopic (OM) images of photonic microspheres: g) PCM-I, h) PCM-II, i) PCM-III, j) PCM-IV, k) PCM-V, l) PCM-VI. Scale bars are 200 μm.

uniform, compact coating as displayed in Figure 2b. The high-magnified SEM image indicates that the glass sphere surface exhibits many spindrift-like bulges (Figure 2b). Particularly, it is observed that the shell coating is grown tightly along the undulating substrate topography resembling those of a pristine glass surface, indicating good conformality due to self-limiting surface chemical reaction of the ALD process.[34,38,39] These observations can be well found in other samples, as evidenced in Figure S3a–e (Supporting Information), further confirming the superior uniformity and conformability. By contrast, conventional sputtering deposition usually causes gradual variation of thickness.[33] Furthermore, the formation of lamellar photonic nanostructures with localized ordering can be clearly observed from the high-magnified SEM image (Figure 2c); the dark and light layers are identified as Al_2O_3 and ZnO lamellae, respectively, as indicated by red arrows (Figure 2c,d and Figure S3a–e). X-ray diffraction (XRD) measurement also validates the formation of wurtzite ZnO and Al_2O_3 (Figure 2d and Figure S4, Supporting Information), indicating the chemical reaction of organometallic precursors with water and thus the formation of covalent bonding between them.[39,40] The thickness of Al_2O_3 layers is measured to be ≈55 nm, while the ZnO lamella thicknesses increase gradually from ≈44 to 135 nm with increasing ALD cycle number from 200 to 700 (Table S1, Supporting Information). These results were further supported by energy-dispersive X-ray spectroscopy (EDS, Figure S5, Supporting Information). According to the above thicknesses and ALD cycles, the average growth rates of Al_2O_3 and ZnO are calculated to be 0.14 and 0.22 nm per cycle, respectively, which matches well with the theoretical values,[36] implying the self-limiting growth of those concentric periodic lamellae.

The microspheres display vibrant metallic reflection colors. In the reflectance spectra for the individual microspheres, it can be seen that each sample contains one principal peak stemmed from first-order diffraction peak of Bragg reflection in visible spectrum (discussed below), and the peak position shifts from 390 to 810 nm with increasing ZnO lamella thickness from 44 to 135 nm (Figure 2e). Remarkably, the black background of the glass microsphere substrate reduces incoherent scattering in the visible spectral range (Figure S6, Supporting Information),[16–17,33] thereby giving rise to structural color with higher saturation. Optical microscopy images directly indicate that these photonic microspheres feature a bright central spot with vibrant structural colors, ranging from violet, blue, green, orange, red, to dark-red, at their top surfaces (Figure 2g–l); there is no distinguishable difference in color between each microsphere of the same sample. As typical examples, PCM-II exhibits a reflective wavelength of 452 nm with a vivid blue appearance, while PCM-IV gives an orange color with a reflective peak located at 721 nm. Note that a second peak is shown at 405 nm for the PCM-VI sample due to the second-order Bragg diffraction peak, which merges with the broad first-order reflective band at 810 nm to produce a mixed dark-red color in human eyes. Under normal incidence, the wavelength λ of 1D photonic crystal is determined by a simplified Bragg diffraction equation: $m\lambda = 2(n_l d_l + n_h d_h)$, where m refers to diffraction order, d_l and d_h represent the periodic thicknesses of low and high refractive material, n_l and n_h denote their refractive indices, respectively. Clearly, the reflection peak wavelength

increases with increasing ZnO thickness. A more standardized expression of the resulting structural colors is plotted in Commission Internationale de L'Eclairage (CIE) chromaticity diagram (Figure 2f), which covers the entire visible spectrum and agrees well with the optical images.

To further verify the structural colors, we compared the experimentally measured wavelengths with the results of numerical simulation (Figure S7 and Table S1, Supporting Information). Finite element method was performed for simulating the reflection spectra of photonic microspheres. The object with concentric 1-dimensional PC shell grown onto a rigid glass microsphere inner core was built, in which the photonic shell has two periods of Al_2O_3/ZnO. To obtain actual refractive indices, Al_2O_3 and ZnO thin films were deposited on silicon wafer under the same ALD condition, from which the refractive indices were measured to be 1.65 and 1.95 for Al_2O_3 and ZnO, respectively. Apparently, the simulation shows that reflection peak wavelength redshifts with increasing ZnO thickness, and matches well with the measured, as listed in Table S1 (Supporting Information). Taking PCM-VI as an example, the thicknesses of the Al_2O_3 and ZnO lamellae are 55 and 135 nm, respectively. Correspondingly, wavelengths of 813 and 339 nm are simulated for the first- and second-order diffraction peaks, respectively. As expected, this result is in good agreement with that of our experimental measurements.

To validate the angle-independence of structural color, we measured orientation-dependent microscopic reflectance spectra of individual microsphere for each sample by tilting a substrate to the right and forward (**Figure 3**a,b), using an angle-resolved spectrum system in micro-region. For measurement, a single microsphere is located in the center of view field, and normal reflective spectra are recorded by selecting the spot area. As expected, the resultant photonic microspheres show orientation-independent structural color. Figure 3a,b and Figures S8a–f and S9a–f (Supporting Information) display normal reflection spectra of rotated microspheres. It can be seen that the reflectance spectra well remain the identical shapes, positions, and intensities; no distinguishable change in the color incurs with increasing tilting angles, due to the uniform growth of concentric photonic shell around the curved surface as aforementioned. Furthermore, the corresponding angle-dependent reflectance spectra were also measured in a mirror-like reflection mode, by varying the angle from 0° to 60°, as illustrated in Figure 3d. Apparently, as the angle increases, the diffractive peak positions of all samples almost remain constant, thus exhibiting the same colors, as shown in Figure 3e and Figure S10a–f (Supporting Information). For example, a microsphere of PCM-II retains the position at around 452 nm giving a constant blue color, indicating negligible angle-dependence of structural color. The macroscopic observation further supports the above measurement, as shown in Figure 3c.[4,16,17] In contrast, those concentric microspheres with long-range ordering of the concentric lamellae in radial orientation exhibit strong angle-dependence,[31] implying the contribution of short-range ordering of the localized concentric structure to the angle-independence of structural color. In addition, the observation of angle-independent structural color in colloidal photonic crystals with short-range ordering further supports the above conclusion. Therefore, these results evidently demonstrate
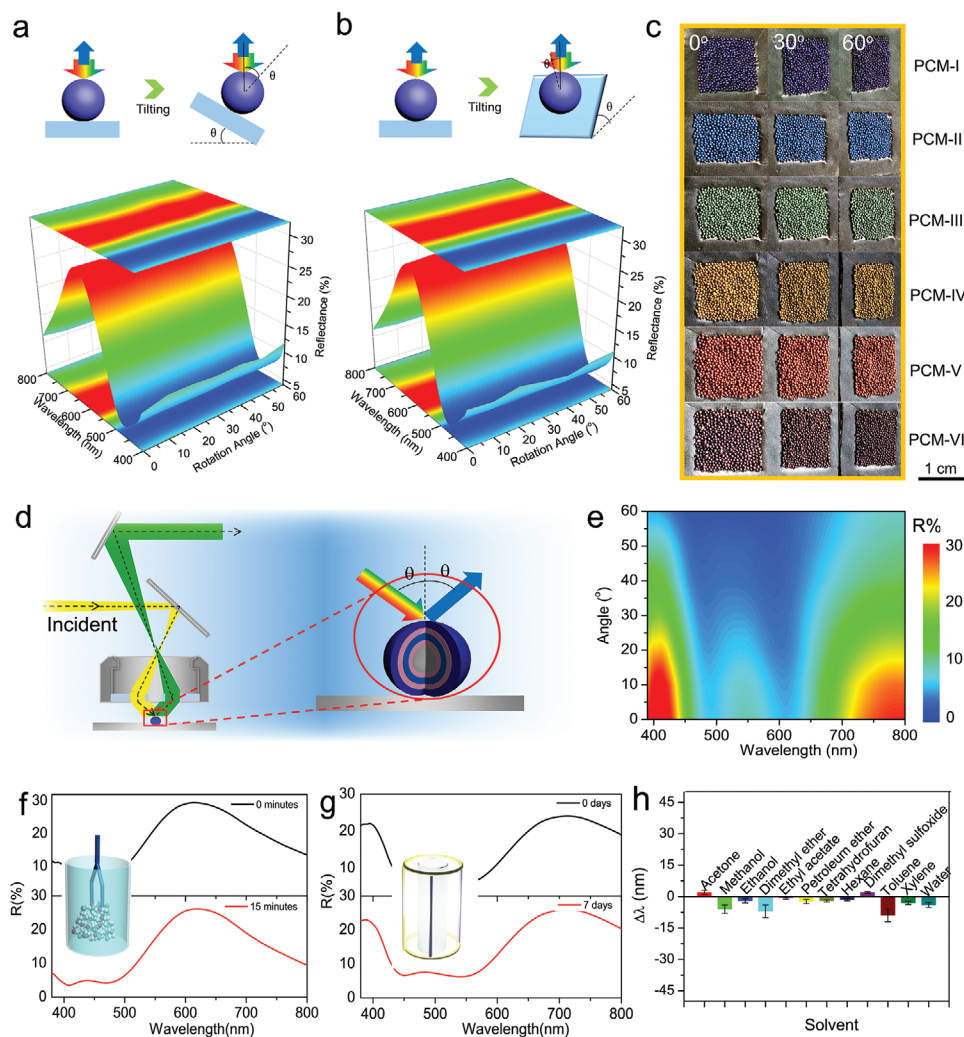
**ADVANCED
SCIENCE NEWS**
www.advancedsciencenews.com

NANO · MICRO
small
www.small-journal.com

Figure 3. Schematic illustrations and orientation-dependent reflection spectra of PCM-IV microsphere measured by tilting a substrate a) right and b) forward. c) Optical images of photonic microspheres under various observing angles. d) Depiction of the setup used to measure angle-dependent reflection spectra from a single photonic microsphere. e) 2D cartoon map of angle-dependent reflection spectra of PCM-II microsphere. f) Reflection spectra of PCM-IV microsphere before and after ball milling in the presence of ZrO₂ bead. Speed: 150 rpm, time: 20 min. g) Reflection spectra of PCM-V microsphere before and after accelerated light-aging test using a Sunlight Climate Tester YG(B)911-V. Temperature: 40 °C, humidity: 50% and irradiance 1.1 W m⁻² at 420 nm, time: 7 continuous days. h) Relative wavelength changes of microsphere under various solvents.

orientation- and angle-independence of the structural colors, which are desirable advantages for practical applications under complex varying lighting and viewing conditions.

The photonic shell is made of robust inorganic ZnO and Al_2O_3 lamellae formed from self-limiting surface reaction via ALD, endowing the photonic microspheres with mechanical robustness, thermal stability, high lightfastness, and resistance to various solvents (Figure 1b). To demonstrate the mechanical robustness, a ball-milling experiment was conducted by adding the PCM-II microspheres into a tube containing ZrO_2 grinding beads (Mohs hardness rating of 9). The microspheres were milled under mechanical stirring at a speed of 150 rpm for 20 min. The reflectance spectra reveal that the photonic microsphere after ball-milling shows unshifted reflection peak compared with the original one, as shown in Figure 3f, indicating the excellent mechanical robustness of structural color due to high mechanical properties and chemical reaction of inorganic

layer, as evidenced in our previous report.[41,42] This robustness is very difficult to achieve in those photonic microspheres reported previously.[15–17] Meanwhile, accelerated light aging measurement reveals that PCM-II photonic microsphere retain their optical performance. As displayed in Figure 3g, no significant variation in color and reflection peaks are shown, since the spectra result from the interaction between light and their physical structures, suggesting their excellent light fastness. In addition, maintaining the same reflectance spectra before and after calcination at 350 °C for 1 h indicates an extreme temperature tolerance (Figure S11, Supporting Information), due to the intrinsic thermal stability of inorganic material. Moreover, solvent resistance is an important parameter for practical applications. Here, we assess the solvent resistance by soaking PCM-II photonic microspheres in water and various organic solvents (including acetone, methanol, ethanol, ether, ethyl acetate, petroleum ether, tetrahydrofuran, dimethyl sulfoxide, hexane,

ADVANCED
SCIENCE NEWS
www.advancedsciencenews.com

NANO · MICRO
small
www.small-journal.com

toluene, and xylene) for 24 h. As expected, the difference in the reflective peak positions is found to vary only in the range of 0.7–9.0 nm (Figure 3h, Figures S12–S23, Supporting Information). Accordingly, the excellent resistance to water and above organic solvents and the merits demonstrated above make the photonic microsphere very promising for long-term practical services under harsh conditions.

The outstanding performances of these photonic microspheres allow their application as robust building blocks for photonic encoding with diverse complexed patterns (Figure 1c). As shown in **Figure 4**a, various photonic micropatterns could be created by manipulating microspheres. It is clearly observed that these photonic micropatterns exhibit distinct shapes with bright color at their top surfaces, under an optical microscope with reflection mode. By assembling microspheres with different colors, a diverse set of encoded multicolored patterns is developed (Figure 4b). Obviously, each microsphere in the multicolored patterns displays a distinguishable central spot with vibrant color, owing to normal Bragg reflection. The multiple combinations of shapes and color choices of the microspheres could yield numerous kinds of photonic patterns for 3D coding.[23,27] For example, as many as 1.6×10^4 hexagonally closed-packed coding patterns can be achieved, when six types of structurally colored microspheres were used (Figure 4b, bottom). Further changing pattern shapes would significantly increase encoding numbers. Moreover, since the photonic microspheres possess the orientation- and angle-independent structural color, the encoded photonic patterns derived from the combination of these spheres enable wide viewing angles, thus offering more reliability and robustness for the subsequent applications.

The microspheres in arranged patterns show colored dots surrounding the bright central spot, forming sub-patterns with more complicated photonic information, as shown in enlarged images (Figure 4c,d and Figure S24, Supporting Information). This phenomenon originates from double reflections of the beam on the surfaces of adjacent photonic microspheres, namely, photonic cross-communication.[25,26,33,43] Specifically, the normal incident beam that impinges to the side of a microsphere at an angle of 45° is first reflected, and then propagates along the horizontal direction of substrate. Subsequently, the beam is reflected secondly by a neighboring microsphere surface to produce colored dots (Figure 4c,d). For photonic patterns composed of microspheres with the same structural color, the color of the surrounding dots is coincident with that of the central spot (Figure 4a,c); this observation is distinct from the character of blue-shift in cholesteric liquid crystal counterparts.[25,26,43] This is because of their aforementioned orientation- and angle-independent reflection (Figure 3 and Figure S10a–f, Supporting Information). As a result, the peak remains constant in the first and second reflections, as illustrated in Figure 4c, producing the same color in the surrounding dots and the central spots. Interestingly, in the case of different structurally colored microspheres, the surrounding dots exhibit an intermediate color of the two microspheres (Figure 4b,d, Figures S24 and S25, Supporting Information). This intermediate color may be attributed to the reflection of the overlapping part between the first and second reflection peaks (Figure 4d). When the beam reflected by first microsphere impinges on the side of neighboring one, only the light located in the photonic stopband of the second microsphere will be reflected, thus giving rise to the intermediate structural color, as illustrated in Figure 4d. It is reasonable considering their broad band reflection (Figure 2e). This fine sub-patterns can be further used as "fingerprint information" of encoded patterns, thus dramatically increasing security level, and enabling deep encryption and anti-counterfeiting. Correspondingly, decoding process could be realized easily by taking optical images. This multicolored encoding strategy with double photonic patterns offers a convenient and reliable tool for anti-counterfeiting.

A series of proof-of-concept experiments were conducted. For example, photonic patterns of "D," "L," "U," and "T" composed of PCM-II, PCM-III, PCM-IV, and PCM-V, respectively, were prepared, as shown in Figure 4e. These photonic patterns exhibit determined shapes and structural colors, accompanying with sub-patterns under an optical microscope. Moreover, such photonic patterns can be further applied to diverse substrates for deep anti-counterfeiting. Figure 4f–i shows the corresponding optical images of photonic patterns which are embedded in pharmaceutical packaging, credit card, key, and cosmetic packaging, respectively. Upon illumination by white light, the patterns are imparted with specific structural colors. At the same time, the "fingerprint information" is also identified, indicating that the photonic microspheres could be used as powerful platform for real-world anti-counterfeiting applications.

By harnessing the inherent pyroelectric and optoelectronic properties of the ZnO layer, our photonic microspheres can serve as building blocks for constructing advanced multifunctional optoelectronic microsensor (Figure 1d). Microsensors have attracted considerable interests because of their miniaturization, intelligence, low-power consumption, and easy integration. In particular, multifunctional microsensors provide multi-parametric sensing capabilities, which simplify device structure and reduce production costs.[40,44–49] As demonstration, a SPCM-based optoelectronic microsensor with triple sensing capabilities, including temperature, infrared (IR) light, and UV light, is developed (**Figure 5**a, see Supporting Information for details). The application of our SPCM-based device as a temperature sensor is investigated first. Figure 5b displays the calibrated current change as a function of temperature in the range of 24–58 °C, which covers the temperature range needed for medical diagnostics of human. The sensor exhibits a good linear relationship with a fitted equation of $\Delta I/I_0 = 8.5 \times T - 214.5$, $\Delta I = I - I_0$, where I and I_0 are the current at a determined temperature (T) and 24 °C, respectively. Accordingly, a temperature sensitivity of 8.5% °C^{-1} is obtained from the slope of above equation, which is higher than many recently reported temperature sensors (0.16–1.8% °C),[50,51] indicating its high sensitivity. This result could be ascribed to the pyroelectric effect of wurtzite ZnO layer (Figure S4, Supporting Information); elevating the temperature induces anisotropic deformation of ZnO material and thus the change of spontaneous polarization.[40,44,45,52] As a result, surface charges are separated and a polarization electric field is produced, thereby increasing the current in external circuit under an applied voltage. In addition, the repeated temperature response between 25 and 50 °C further confirms cyclic stability (Figure 5c).
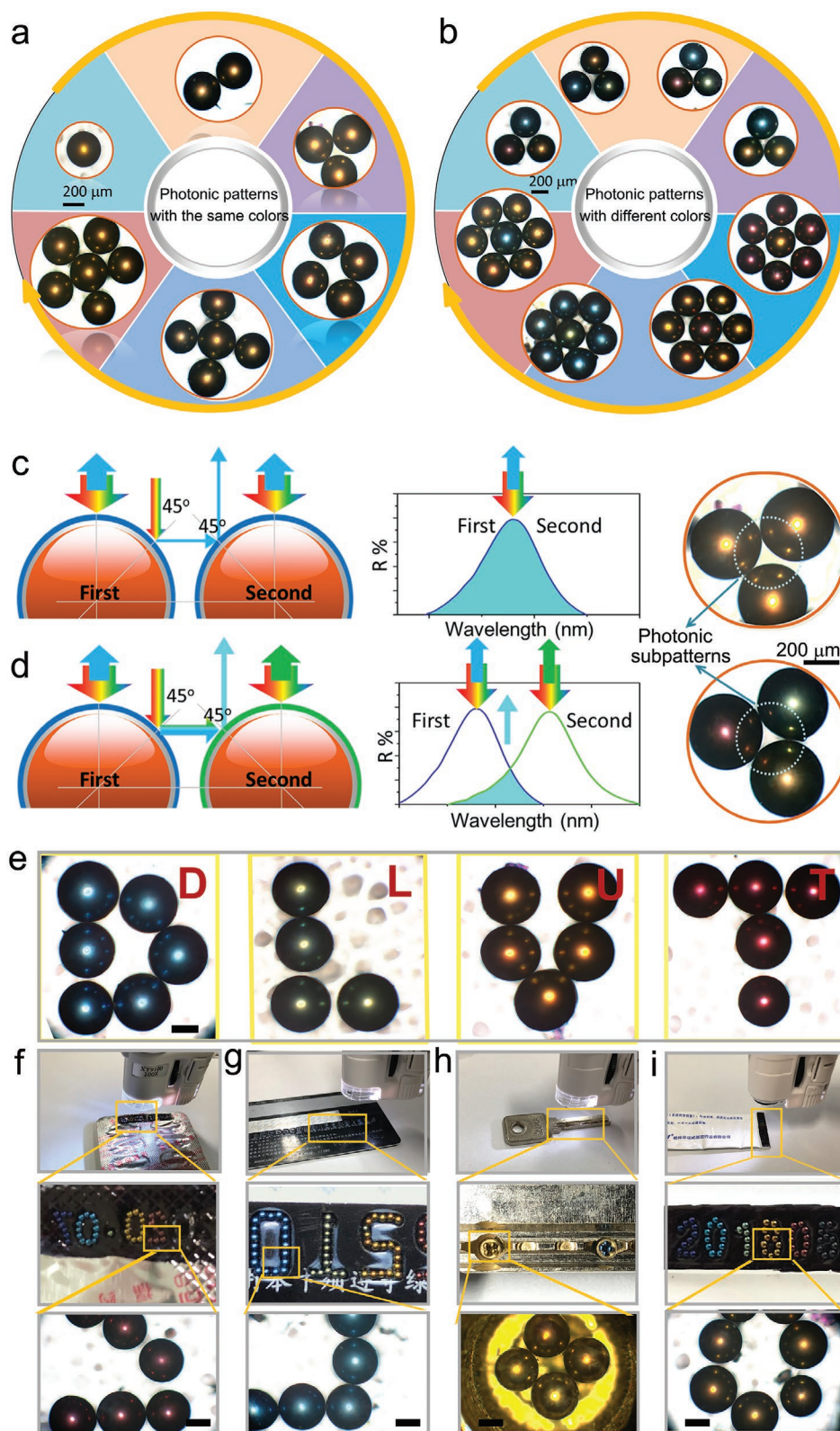
Figure 4. Applications of photonic microspheres. Photonic patterns composed of microspheres with the a) same and b) different structural colors. c) Schematic illustrations showing beam paths, reflection, and optical images for photonic cross-communication between two neighboring microspheres with the (c) same and d) different structural colors. e) OM images of the microsphere array with sub-patterns. Capitalized initial letters for each word of "DaLian University of Technology." Scale bar is 200 μm f–i) Anti-counterfeiting capability of the photonic patterns: various substrates used in experiments at macro (top row) and micro (bottom row) levels. Scale bars are 200 μm.
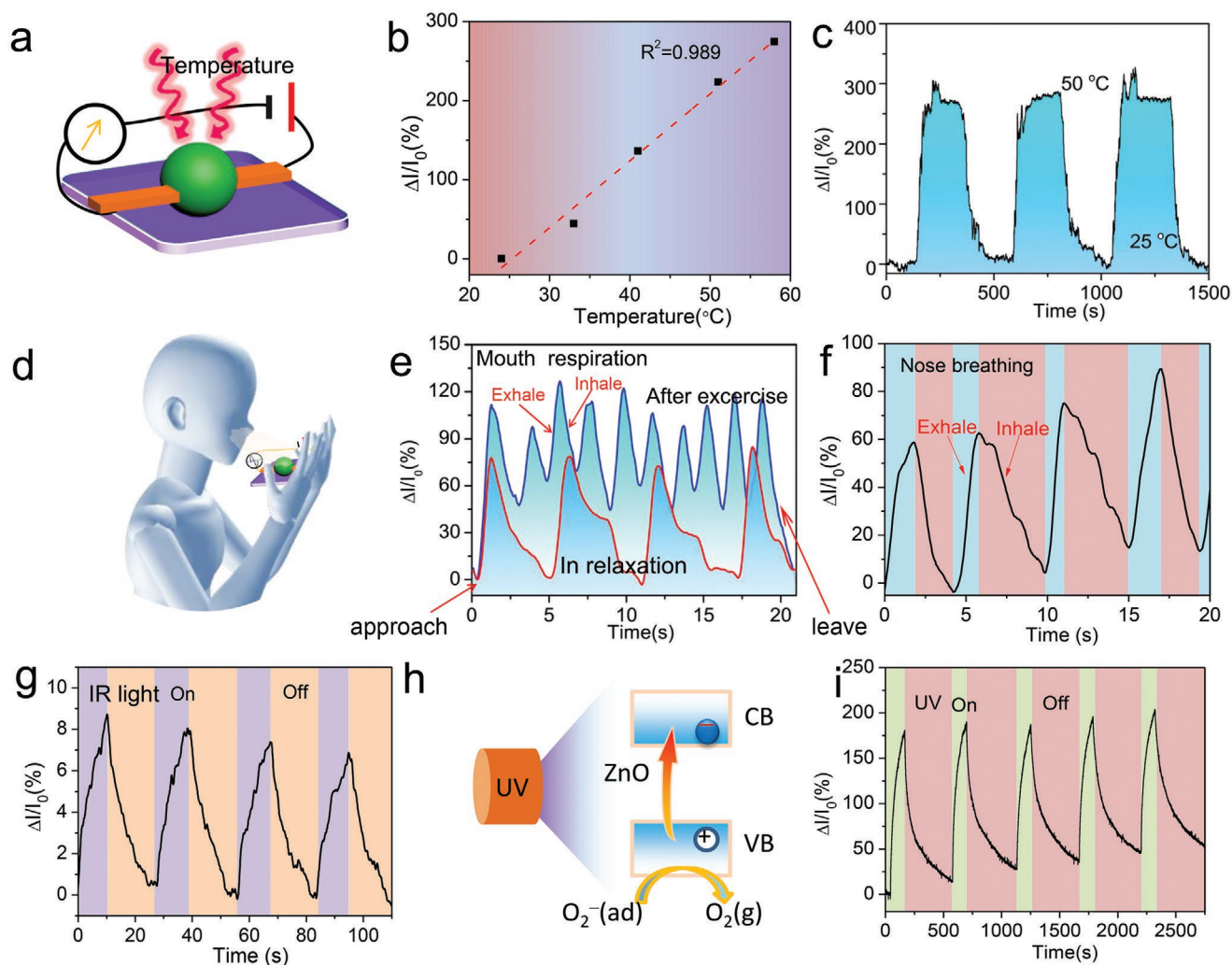
Figure 5. The applications of photonic microspheres as a multifunctional microsensor. a) Illustration showing the structure of the SPCM-based sensor with triple sensations. For performance measurement, a voltage of 0.5 V is applied. b) Calibration of the current change as a function of temperature. c) Cyclic test of the sensor between room temperature (25 °C) and 55 °C. d) Schematic diagram and response of the sensor to e) mouth respiration before and after intense exercise and f) nose breathing. g) Response of the sensor to 980 nm IR light. h) UV sensing mechanism and i) response of the sensor under 365 nm UV exposure.

By virtue of the sensitivity and measurable temperature range, the SPCM-based sensor can be used to detect physiological signals by monitoring subtle thermal fluctuation. Respiration is an important indicator reflecting healthy level of human body.[53,54] The SPCM-based sensor is capable of detecting respiration, because inhalation and exhalation through mouth and nose usually induce temperature changes (Figure 5e,f). For example, a reproducible and steady electrical signal response is generated through the change of temperature, when a volunteer approaches the sensor. There is a steady and continuous signal change accompanying with mouth breathing in a relaxed state. By contrast, much denser and stronger signal peaks are observed after intense exercise (Figure 5e). This is due to the larger thermal changes induced by deep breathing and higher body temperature after intense exercise.[48,53] It should be mentioned that the electronic signal change does not return to nearly zero and remains at ≈45%, which is substantially higher than that of the plot of the control experiment. This is mainly

caused by residual temperature change and heat emission from human body,[40] which still acts on the sensor until the person leaves from it. The excellent respiration recognition ability enables this sensor to have great potential in wearable electronics for health tracking and medical diagnosis, by continuously monitoring the temperature.[48,55,56]

Further taking advantage of the pyroelectric and photothermal effects, the SPCM-based sensor can be used for IR sensing. Figure 5g displays the response of the sensor when it is cyclically illuminated under 980 nm IR light; the sensor shows a good repeatability, revealing its ability to detect IR light, and is promising for IR overheating warning device application. Moreover, we also demonstrate the UV sensibility of the device. According to previous research, ZnO is an appealing material for UV detector. The photoelectric effect and oxygen adsorption/desorption are responsible for the UV sensibility (Figure 5i).[40] Typically, oxygen molecules adsorbed on the ZnO surface trap free electrons, forming O^{2-} and reducing

conductivity.[40,57] Upon UV exposure, photogenerated holes will react with O^{2-} to form O_2 and then release it. This process enhances the conductivity, which together with photogenerated free electrons increases the current.[40,57] Here, the SPCM-based sensor displays a distinctive and repeatable signal pattern during cyclic UV exposures, as shown in Figure 5h, exhibiting appealing applications in UV early-warning devices.

In conclusion, we have developed a new kind of robust, multifunctional all-inorganic photonic microspheres by designing the localized concentric ordering structure and introducing chemical interaction, and demonstrated their applications for multicolored patterns encoding and multiple sensory microsensor. The microspheres show orientation- and angle-independent structural colors owing to unique localized concentric structure. Notably, taking advantages of good mechanical properties of inorganic lamellae and the chemical covalent bonding interaction formed during ALD process, these microspheres exhibit superior mechanical robustness, thermal stability, light fastness, and excellent solvent tolerance. By using photonic microspheres as building blocks, we constructed variously encoded photonic patterns with substantial coding level. Remarkably, double reflections of beam among the microspheres create complex photonic sub-patterns that act as "fingerprint information," allowing for deep encryption and high-level anti-counterfeiting applications, which are rarely reported in conventional encoded patterns. Moreover, by taking advantage of the pyroelectric and optoelectronic properties of the ZnO layer, we successfully fabricate a novel SPCM-based sensor, which shows triple electrical sensing capability to temperature, IR and UV, demonstrating appealing applications for thermal activities monitoring of human body, and early IR-overheating and UV warning.

Besides, we believe this class of photonic microsphere has great potential as a new structurally colored pigment for outdoor painting and reflective display considering their superior robustness, stability, and solvent resistance; by introducing magnetic microcores, magnetoresponsive photonic microsphere could also be produced for magnetically controlled motion, separation, and display. Notably, due to the small size and low power consumption of sensing element, SPCM-based microsensor can be further integrated into emerging wearable electronics and diverse smart devices for healthcare and consumer applications. We anticipate that these demonstrated photonic microspheres will benefit broader photonic and electronic applications beyond these examples.

Supporting Information

Supporting Information is available from the Wiley Online Library or from the author.

Acknowledgements

Conflict of Interest

The authors declare no conflict of interest.

Keywords

[1] Y. Wang, M. Li, E. Colusso, W. Li, F. G. Omenetto, *Adv. Opt. Mater.* **2018**, *6*, 1800066.

[2] H. Tan, Q. Lyu, Z. Xie, M. Li, K. Wang, K. Wang, B. Xiong, L. Zhang, J. Zhu, *Adv. Mater.* **2019**, *31*, 1805496.

[3] E. S. A. Goerlitzer, R. N. Klupp Taylor, N. Vogel, *Adv. Mater.* **2018**, *30*, 1706654.

[4] M. Kolle, S. Lee, *Adv. Mater.* **2018**, *30*, 1702669.

[5] X. Wu, R. Hong, J. Meng, R. Cheng, Z. Zhu, G. Wu, Q. Li, C. F. Wang, S. Chen, *Angew. Chem.* **2019**, *58*, 13556.

[6] J. Liao, C. Zhu, B. Gao, Z. Zhao, X. Liu, L. Tian, Y. Zeng, X. Zhou, Z. Xie, Z. Gu, *Adv. Funct. Mater.* **2019**, *29*, 1902954.

[7] J. Zhang, Z. Zhu, Z. Yu, L. Ling, C. F. Wang, S. Chen, *Mater. Horiz.* **2019**, *6*, 7.

[8] Y. Zhang, Y. Wang, H. Wang, Y. Yu, Q. Zhong, Y. Zhao, *Small* **2019**, *15*, 1902198.

[9] J. Liu, L. Wan, M. Zhang, K. Jiang, K. Song, J. Wang, T. Ikeda, L. Jiang, *Adv. Funct. Mater.* **2017**, *27*, 1605221.

[10] S. Y. Lee, J. S. Lee, S. H. Kim, *Adv. Mater.* **2019**, *31*, 1901398.

[11] J. Liu, Z. Xie, Y. Shang, J. Ren, R. Hu, B. Guan, J. Wang, T. Ikeda, L. Jiang, *ACS Appl. Mater. Interfaces* **2018**, *10*, 6701.

[12] M. Quan, B. Yang, J. Wang, H. Yu, X. Cao, *ACS Appl. Mater. Interfaces* **2018**, *10*, 4243.

[13] S. H. Kim, J. G. Park, T. M. Choi, V. N. Manoharan, D. A. Weitz, *Nat. Commun.* **2014**, *5*, 3068.

[14] T. M. Choi, J. G. Park, Y. S. Kim, V. N. Manoharan, S. H. Kim, *Chem. Mater.* **2015**, *27*, 1014.

[15] L. Shang, Y. Cheng, Y. Zhao, *Chem. Rev.* **2017**, *117*, 7964.

[16] Z. H. Ming Xiao, Z. Wang, Y. Li, A. D. Tormo, N. L. Thomas, B. Wang, N. C. Gianneschi, M. D. Shawkey, A. Dhinojwala, *Sci. Adv.* **2017**, *3*, 1701151.

[17] Y. Zhao, L. Shang, Y. Cheng, Z. Gu, *Acc. Chem. Res.* **2014**, *47*, 3632.

[18] S. J. Yeo, K. J. Park, K. Guo, P. J. Yoo, S. Lee, *Adv. Mater.* **2016**, *28*, 5268.

[19] D. Zhang, J. Liu, B. Chen, Y. Zhao, J. Wang, T. Ikeda, L. Jiang, *ACS Nano* **2018**, *12*, 12149.

[20] Y. Liu, L. Shang, H. Wang, H. Zhang, M. Zou, Y. Zhao, *Mater. Horiz.* **2018**, *5*, 979.

[21] L. Shang, F. Fu, Y. Cheng, H. Wang, Y. Liu, Y. Zhao, Z. Gu, *J. Am. Chem. Soc.* **2015**, *137*, 15533.

[22] Y. Zhao, Z. Xie, H. Gu, L. Jin, X. Zhao, B. Wang, Z. Gu, *NPG Asia Mater.* **2012**, *4*, 25.

[23] J. Hou, M. Li, Y. Song, *Angew. Chem.* **2018**, *57*, 2544.

[24] L. Li, Z. Chen, C. Shao, L. Sun, Y. Zhao, *Adv. Funct. Mater.* **2020**, *30*, 1906353.

[25] S. S. Lee, S. K. Kim, J. C. Won, Y. H. Kim, S. H. Kim, *Angew. Chem.* **2015**, *54*, 15266.

[26] S. S. Lee, H. J. Seo, Y. H. Kim, S. H. Kim, *Adv. Mater.* **2017**, *29*, 1606894.

[27] F. Dong, W. Chu, *Adv. Mater.* **2019**, *31*, 1804921.

[28] L. Shang, F. Shangguan, Y. Cheng, J. Lu, Z. Xie, Y. Zhao, Z. Gu, *Nanoscale* **2013**, *5*, 9553.

[29] S. H. Kim, S. J. Jeon, G. R. Yi, C. J. Heo, J. H. Choi, S. M. Yang, *Adv. Mater.* **2008**, *20*, 1649.

[30] T. M. Choi, G. H. Lee, Y. S. Kim, J. G. Park, H. Hwang, S. H. Kim, *Adv. Mater.* **2019**, *31*, 1900693.

[31] D. P. Song, T. H. Zhao, G. Guidetti, S. Vignolini, R. M. Parker, *ACS Nano* **2019**, *13*, 1764.

[32] Y. Yang, H. Kim, J. Xu, M. S. Hwang, D. Tian, K. Wang, L. Zhang, Y. Liao, H. G. Park, G. R. Yi, X. Xie, J. Zhu, *Adv. Mater.* **2018**, *30*, 1707344.

[33] S. Y. Lee, J. Choi, J. R. Jeong, J. H. Shin, S. H. Kim, *Adv. Mater.* **2017**, *29*, 1605450.

[34] W. Niu, X. Li, S. K. Karuturi, D. W. Fam, H. Fan, S. Shrestha, L. H. Wong, A. I. Tok, *Nanotechnology* **2015**, *26*, 064001.

[35] S. M. Lee, E. Pippel, U. Gosele, C. Dresbach, Y. Qin, C. V. Chandran, T. Brauniger, G. Hause, M. Knez, *Science* **2009**, *324*, 488.

[36] R. H. Vervuurt, B. Karasulu, M. A. Verheijen, W. E. Kessels, A. A. Bol, *Chem. Mater.* **2017**, *29*, 2090.

[37] L. T. Su, S. K. Karuturi, J. Luo, L. Liu, X. Liu, J. Guo, T. C. Sum, R. Deng, H. J. Fan, X. Liu, A. I. Tok, *Adv. Mater.* **2013**, *25*, 1603.

[38] S. K. Karuturi, J. Luo, C. Cheng, L. Liu, L. T. Su, A. I. Tok, H. J. Fan, *Adv. Mater.* **2012**, *24*, 4157.

[39] S. D. Elliott, G. Dey, Y. Maimaiti, H. Ablat, E. A. Filatova, G. N. Fomengia, *Adv. Mater.* **2016**, *28*, 5367.

[40] X. Liao, Q. Liao, Z. Zhang, X. Yan, Q. Liang, Q. Wang, M. Li, Y. Zhang, *Adv. Funct. Mater.* **2016**, *26*, 3074.

[41] W. Niu, L. Zhang, Y. Wang, S. Zhang, *J. Mater. Chem. C* **2019**, *7*, 3463.

[42] W. Niu, L. Zhang, Y. Wang, Z. Wang, K. Zhao, S. Wu, S. Zhang, A. I. Y. Tok, *ACS Appl. Mater. Interfaces* **2019**, *11*, 32261.

[43] J. Noh, H.-L. Liang, I. Drevensek-Olenik, J. P. F. Lagerwall, *J. Mater. Chem. C* **2014**, *2*, 806.

[44] W. R. K. Illeperuma, J.-Y. Sun, Z. Suo, J. J. Vlassak, *Soft Matter* **2013**, *9*, 8504.

[45] S. H. Yuki Yamamoto, D. Yamamoto, W. Honda, T. Arie, S. Akita, K. Takei, *Sci. Adv.* **2016**, *2*, 1601473.

[46] T. Yamada, Y. Hayamizu, Y. Yamamoto, Y. Yomogida, A. Izadi-Najafabadi, D. N. Futaba, K. Hata, *Nat. Nanotechnol.* **2011**, *6*, 296.

[47] Y. Gao, J. Song, S. Li, C. Elowsky, Y. Zhou, S. Ducharme, Y. M. Chen, Q. Zhou, L. Tan, *Nat. Commun.* **2016**, *7*, 12316.

[48] M. Zhang, C. Wang, H. Wang, M. Jian, X. Hao, Y. Zhang, *Adv. Funct. Mater.* **2017**, *27*, 1604795.

[49] Y. Tai, G. Lubineau, *Adv. Funct. Mater.* **2016**, *26*, 4078.

[50] J. Guo, B. Zhou, C. Yang, Q. Dai, L. Kong, *Adv. Funct. Mater.* **2019**, *29*, 1902898.

[51] B. Dong, B. Cao, Y. He, Z. Liu, Z. Li, Z. Feng, *Adv. Mater.* **2012**, *24*, 1987.

[52] S. K. Karuturi, C. Cheng, L. Liu, L. Tat Su, H. J. Fan, A. I. Y. Tok, *Nano Energy* **2012**, *1*, 322.

[53] C. Wang, X. Li, E. Gao, M. Jian, K. Xia, Q. Wang, Z. Xu, T. Ren, Y. Zhang, *Adv. Mater.* **2016**, *28*, 6640.

[54] M. Amjadi, K. U. Kyung, I. Park, M. Sitti, *Adv. Funct. Mater.* **2016**, *26*, 1678.

[55] L. Q. Tao, K. N. Zhang, H. Tian, Y. Liu, D. Y. Wang, Y. Q. Chen, Y. Yang, T. L. Ren, *ACS Nano* **2017**, *11*, 8790.

[56] I. You, B. Kim, J. Park, K. Koh, S. Shin, S. Jung, U. Jeong, *Adv. Mater.* **2016**, *28*, 6359.

[57] Q. H. Li, T. Gao, Y. G. Wang, T. H. Wang, *Appl. Phys. Lett.* **2005**, *86*, 123117.